

Six-dimensional quasiclassical and quantum dynamics of H₂ dissociation on the c(2 × 2)-Ti/Al(100) surface

Jian-Cheng Chen,^{1,a)} Juan Carlos Juanes-Marcos,^{1,2} Sylvain Woittequand,¹ Mark F. Somers,¹ Cristina Díaz,^{1,3} Roar A. Olsen,^{1,4} and Geert-Jan Kroes¹

¹*Leiden Institute of Chemistry, Gorlaeus Laboratories, Leiden University, P.O. Box 9502, 2300 RA Leiden, The Netherlands*

²*Department of Chemistry, University of Nevada Las Vegas, 4505 South Maryland Parkway, Las Vegas, Nevada 89154-4003, USA*

³*Departamento de Química Módulo 13, Universidad Autónoma de Madrid, 28049 Madrid, Spain*

⁴*Akershus University College, P.O. Box 423, N-2001 Lillestrøm, Norway*

(Received 14 December 2010; accepted 28 February 2011; published online 18 March 2011)

Based on a slab model of H₂ dissociation on a c(2 × 2) structure with Ti atoms in the first and third layers of Al(100), a six-dimensional (6D) potential energy surface (PES) has been built. In this PES, a molecular adsorption well with a depth of 0.45 eV is present in front of a barrier of height 0.13 eV. Using this PES, H₂ dissociation probabilities are calculated by the classical trajectory (CT), the quasiclassical trajectory (QCT), and the time-dependent wave-packet (TDWP) method. The QCT study shows that trajectories can be trapped by the molecular adsorption well. Higher incident energy can lead to direct H₂ dissociation. Vibrational pre-excitation is the most efficient way to promote direct dissociation without trapping. We find that both rotational and vibrational excitation have efficacies close to 1.0 in the entire range of incident energies investigated, which supports the randomization in the initial conditions making the reaction rate solely dependent on the total (internal and translational) energy. The H₂ dissociation probabilities from quantum dynamics are in reasonable agreement with the QCT results in the energy range 50–200 meV, except for some fluctuations. However, the TDWP results considerably exceed the QCT results in the energy range 200–850 meV. The CT reaction probabilities are too low compared with the quantum dynamical results. © 2011 American Institute of Physics. [doi:10.1063/1.3567397]

I. INTRODUCTION

Plausible explanations of the elementary reaction steps and the corresponding reaction dynamics are key to understanding the complex chemical reactions in hydrogen storage materials, e.g., sodium alanate (NaAlH₄).¹ In a previous study of H₂ reacting on Ti/Al(100) surfaces,² it was found that the most realistic model promoting H₂ dissociation is a one monolayer (ML) Ti covered c(2 × 2)-Ti/Al(100) structure, with Ti atoms in the first and third layers. This model has a minimum energy path (MEP) with a late barrier of only 0.13 eV height at a H–H distance of 1.50 Å, and a deep molecular adsorption well with a depth of 0.45 eV in front of the barrier at a H–H distance of 0.82 Å. Such a molecular adsorption well could lead to sticking and/or trapping of the H₂ molecules on the Ti/Al(100) surface. Processes which can contribute to trapping of H₂ in the molecular adsorption well are energy transfer from translation to rotation (also called rotation-mediated selective adsorption³), energy transfer to motion of H₂ parallel to the surface (corrugation mediated selective adsorption⁴), energy transfer to phonons, and energy transfer to electron–hole pair excitations.⁵ In order to determine to what extent these processes may contribute to sticking of H₂ at the temperatures (50–150 °C) relevant to the uptake and release of hydrogen by NaAlH₄, reaction

probabilities from (quasi)classical or quantum dynamics are needed. The aim of the present work is to investigate the dynamics of the H₂ + Ti/Al(100) reaction from this point of view.

For the analogous H₂ + Ni(100) reaction, which has a shallow molecular adsorption well with a depth of 0.13 eV,⁶ it is justified to treat the dissociation dynamics as a direct process and ignore the molecular adsorption at sufficiently high surface temperatures. Therefore, at high surface temperature only the barrier to dissociation referenced to the gas phase is important. However, at low surface temperature the reaction proceeds through a molecularly adsorbed intermediate, which may be thought of as a stable chemical species. In the latter case, the barrier relevant to the kinetics is the barrier to dissociation referenced to the molecular adsorption well. Reactions proceeding over deep potential energy wells can be treated statistically, if the intermediates are sufficiently long lived.⁷ In this case, a treatment of the formation and decay of the intermediates into reactant and product channels may be enough to give satisfactory results.^{8,9}

Increasing interest in the role of rotational and vibrational energy in promoting the molecule–surface reactivity is driven by the development of new theoretical methods and experimental tools allowing a more detailed insight into the details of a reaction.^{10,11} One of the widely studied systems, H₂ (D₂) + Cu(111) (Refs. 12–18, and 19) is a late barrier system like the system under investigation here. H₂ (D₂) shows a

^{a)}Electronic mail: jcheng@chem.leidenuniv.nl.

preference for reaction in the helicopter approach (a positive rotational quadrupole alignment parameter)^{19–21} to the Cu(111) surface, which indicates that there is a steric effect in the dynamics. Both experimental^{16,17} and theoretical¹⁹ studies show that this system has rotational and vibrational efficacies of 0.40 and 0.65, respectively. Thus, the statistical model²² with a randomization of the initial conditions cannot be applied to this direct reaction. One question addressed here is whether the same conclusion can be drawn for the late barrier system $\text{H}_2 + \text{Ti}/\text{Al}(100)$, which has a deep molecular adsorption well in front of the barrier.

The Born–Oppenheimer (BO) approximation has been found to accurately describe the dissociation of H_2 on metal surfaces,²³ because H_2 has a low electron affinity and the net charge transfer is almost zero during the process of dissociation.^{2,23,24} Thus, we neglect the electron–hole pair excitation. Due to the mismatch between the mass of H_2 and the surface Ti and Al atoms, the energy transfer from the molecule to the metal surface should be small and unlikely to influence the scattering result. Therefore, the $\text{Ti}/\text{Al}(100)$ slab can be fixed during the process of H_2 dissociation, and we only consider the motion in the six degrees of freedom (DOFs) on the ground state potential energy surface (PES).

Theoretical progress in gas–surface reaction dynamics^{11,25–31} combined with super computer facilities³² make six-dimensional (6D) quantum dynamics calculations of H_2 –surface reaction dynamics possible. Six-dimensional quantum dynamics has been successfully implemented to address the dissociative chemisorption of H_2 on Pd(100) (Refs. 25 and 33), Pd(110) (Ref. 34), Rh(100) (Ref. 33), Cu(100) (Refs. 30 and 35), Cu(111) (Refs. 18, 19, 26, and 28), Pt(111) (Refs. 23 and 36), Pt(211) (Ref. 37), Pd(111) (Ref. 38), Ru(0001) (Ref. 39), NiAl(110) (Refs. 40), and on sulfur-precovered Pd(100) (Ref. 41) and CO-precovered Ru(0001) (Ref. 42).

Based on a slab model of one ML Ti covered $\text{Ti}/\text{Al}(100)$ surface,² a 6D PES has been built by the density functional theory (DFT) (Refs. 43 and 44). Both the quantum and quasiclassical dynamics are calculated on it. Our results show that the H_2 dissociation probabilities obtained from quantum dynamics and quasiclassical dynamics agree well with each other in the low incident energy range, except that the quantum probability has many peaks (associated with the opening up of new rovibrational states or resonances). However, the quantum probability is higher than the quasiclassical one up to 30.0% at incident energies above 0.30 eV.

The layout of this paper is as follows. The methodology and numerical details are presented in Sec. II, in which Sec. II A describes electronic structure calculations by DFT, Sec. II B describes the building of the 6D PES, Sec. II C describes the classical trajectory (CT) and quasiclassical trajectory (QCT) calculations, and Sec. II D describes the time-dependent wave-packet (TDWP) calculations. Results are presented and discussed in Sec. III. Specifically, Sec. III A shows the location of the data points and cuts through the PES. Section III B focuses on the H_2 dissociation probability calculated by QCT. In Sec. II C, comparisons of the CT,

QCT, and TDWP results are presented. Finally, conclusions and an outlook are presented in Sec. IV.

II. METHODOLOGY AND NUMERICAL DETAILS

A. Electronic structure calculations and slab model

The DFT code DACAPO (Ref. 45) is used to study H_2 dissociation on the one ML $c(2 \times 2)$ - $\text{Ti}/\text{Al}(100)$ slab model with Ti atoms in the first and third layers. The PW91 functional,⁴⁶ which has been shown to give reasonably good results for H_2 dissociating on the NiAl(110) alloy surface,^{40,47} is employed to describe the exchange–correlation energy of the electrons. The ion cores are described by ultrasoft pseudopotentials,⁴⁸ with core cutoff radii of $r_c^{\text{H}} = 0.46 \text{ \AA}$, $r_c^{\text{Al}} = 0.84 \text{ \AA}$, and $r_c^{\text{Ti}} = 1.16 \text{ \AA}$. A plane wave basis set is used for the electronic orbitals, with a cutoff energy of 350 eV. The Brillouin zone is sampled by the Monkhorst–Pack⁴⁹ method, using a set of $6 \times 6 \times 1$ k -points. In the Z direction (perpendicular to the surface, see Fig. 1), a vacuum layer of 12.0 \AA was placed between the slabs to avoid artificial interactions caused by the periodic boundary conditions. The lattice constant of the surface unit cell is $a = 4.04 \text{ \AA}$, and more details of the slab structure can be found in Ref. 2.

A three-layer $\text{Ti}/\text{Al}(100)$ slab model is employed in this work to study the H_2 dissociation dynamics (see Fig. 1). Using a (2×2) unit cell, although the interlayer distance between the first-layer Ti and the third-layer Ti is compressed from 3.80 \AA in the four-layer model to 3.67 \AA in the three-layer model after relaxation, our convergence tests show that the H_2 geometries in the molecular adsorption well and at the barrier in this three-layer model are quite similar (difference is less than 0.05 \AA) to the previous four-layer slab model results² using a plane wave cutoff energy of 400 eV and a $12 \times 12 \times 1$ k -point sampling. Most importantly, using this three-layer model, the depth of the molecular adsorption well and the barrier height are 0.43 and 0.13 eV, respectively (converged values calculated with the four-layer slab model are 0.45 and 0.13 eV, respectively). These approximations (using less layers and k -points, and a smaller plane wave cutoff energy) save considerable CPU time in calculating the second-order derivatives for the Hessian matrix, as required to build a 6D PES for the $\text{H}_2 + \text{Ti}/\text{Al}(100)$ reaction (discussed in the next Section, II B). Forward differencing with a hydrogen atomic displacement distance of 0.01 \AA is used to calculate the Hessian. On the basis of tests performed with these parameters, the DFT potential energies are converged to within 5.0×10^{-2} eV.

Our tests also show that the PW91 functional gives results similar to the Perdew–Burke–Ernzerhof (PBE) functional,⁵⁰ which is expected because the PBE functional was designed to reproduce PW91 energies.⁵⁰ We also tested the revised Perdew–Burke–Ernzerhof (RPBE) functional⁵¹ and found that it typically gives higher barriers than the PW91 functional, by about 0.25 eV. This is in accordance with recent theoretical³⁹ and experimental⁵² works on $\text{H}_2 + \text{Ru}(0001)$, $\text{H}_2 + \text{Cu}(111)$ (Ref. 18), N_2 on W(100), and W(110) surfaces,⁵³ where the RPBE dissociation barrier heights were likewise larger than the PW91 barrier heights, and the realistic barrier heights probably fall in between the PW91 and RPBE values.¹⁸

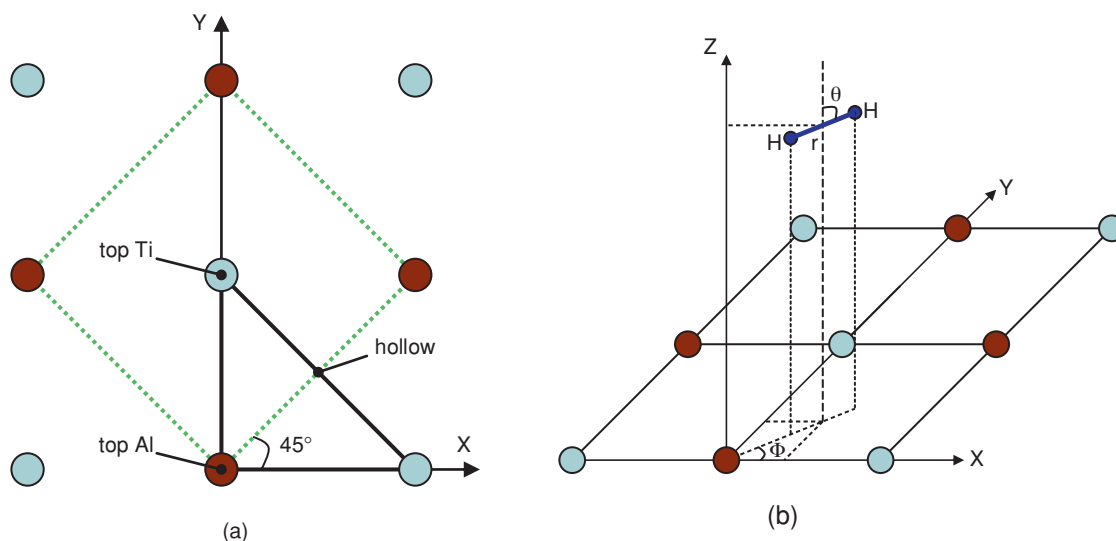


FIG. 1. (a) (2×2) surface unit cell of Ti/Al(100) with lattice constant $a = 4.04 \text{ \AA}$. The brown and blue spheres represent Al and Ti atoms, respectively. The isosceles right triangle (including three boundaries) in black color formed by two Ti atoms and one Al atom, is the area used for adding Grow data points and for the implementation of the quasiclassical simulation. Once the process of adding points to the data set is finished, the potential is set up on the $(\sqrt{2} \times \sqrt{2})$ unit cell (dotted green square area) by using symmetric operations. (b) The coordinates used for H₂ + Ti/Al(100): the H–H atomic distance r , the position of the H₂ COM over the alloy surface (X, Y, Z) , the polar angle θ , and the azimuthal angle ϕ .

B. Modified Shepard (MS) interpolation method and “growing” of the six-dimensional PES

To obtain a global PES, we have used a MS interpolation procedure^{54–57} initially developed by Collins and co-workers for gas phase reactions, and later adapted for studying the molecule–surface dissociative chemisorption reaction.⁵⁸ The procedure of the application of the MS interpolation is informally known as the “Grow” method,^{54–57} in which the energies of the data points are obtained from the slab model mentioned above by DFT. The locations of these data points are centered on the dynamically interesting regions, i.e., the most frequently visited regions by quasiclassical trajectories. The MS interpolation method is efficient and accurate enough^{59,60} compared with the corrugation reducing procedure developed by Busnengo and co-workers.^{61,62}

For 6D and higher dimensionality molecule–surface systems, MS interpolation is an efficient method to get accurate descriptions of molecule–surface interaction potential energy surfaces. Successful applications of the MS method to dissociative chemisorption of a molecule on a metal surface have been demonstrated for a number of examples, such as N₂ + Ru(0001) (Refs. 63 and 64), H₂ + Pt(111) (Ref. 58), H₂ + Pd(111) (Ref. 65), H₂ on CO-precovered Ru(0001) (Ref. 42), and CH₄ + Ni(111) systems (Refs. 66 and 67).

The PES is constructed using inverse interatomic distances $Q_i = 1/R_i$, which give a better mathematical behavior than the interatomic distances R_i when two atoms come close to each other.⁵⁷ For a system with N atoms, the number of interatomic distances is given by $N(N - 1)/2$. Thus, in the system of H₂ + Ti/Al(100), $N = 5$ atoms are required (two hydrogen and three frozen surface atoms) to represent the six H₂ DOFs, using two Ti atoms and one Al atom that form an isosceles right triangle.

According to the MS interpolation method, the potential at a given configuration \mathbf{Q} , in the vicinity of the data point

$\mathbf{Q}(i)$, is given by a second-order Taylor expansion $T_i(\mathbf{Q})$:

$$T_i(\mathbf{Q}) = V[\mathbf{Q}(i)] + \sum_{k=1}^{3N-6} [\xi_k - \xi_k(i)] \left. \frac{\partial V}{\partial \xi_k} \right|_{\mathbf{Q}=\mathbf{Q}(i)} + \frac{1}{2} \sum_{k=1}^{3N-6} \sum_{j=1}^{3N-6} [\xi_k - \xi_k(i)][\xi_j - \xi_j(i)] \left. \frac{\partial^2 V}{\partial \xi_k \partial \xi_j} \right|_{\mathbf{Q}=\mathbf{Q}(i)}. \quad (1)$$

The value of the potential energy at the data point $\mathbf{Q}(i)$, $V[\mathbf{Q}(i)]$, and the gradients with respect to ξ at this point are calculated analytically with DFT. The second derivatives of the potential are calculated using numerical forward finite differences of the gradients, displacing the H atoms by 0.01 \AA .

The MS interpolation gives the potential energy at any configuration \mathbf{Q} as a weighted average of the Taylor expansion terms $T_i(i = 1, \dots, N_{\text{data}})$ calculated from each of the N_{data} data points presented in the PES data set and all symmetry equivalent points:

$$V(\mathbf{Q}) = \sum_{g \in G} \sum_{i=1}^{N_{\text{data}}} w_{g \circ i}(\mathbf{Q}) T_{g \circ i}(\mathbf{Q}). \quad (2)$$

In Eq. (2), G is the symmetry subgroup of the system and $g \circ i$ denotes the transformation of the i th data point by the group element g . The symmetry of the system is taken into account by summing over the data points in the PES data set and the symmetry equivalent points. The nuclear permutation subgroup, C_{2v} is effectively used for the H₂ + Ti/Al(100) system [see the isosceles right triangle with two Ti atoms and one Al atom mentioned above in Fig. 1(a)], although the full symmetry should be C_{4v} . To take into account the full C_{4v} surface symmetry, the number of interatomic distances to be considered should be increased by introducing more surface atoms

into the representation of PES by the Taylor expansion in Eq. (1), also see Fig. 1.

An advantage of the MS interpolation method is that the sampling of data points can be performed nonuniformly over the configuration space. This can be done so that only the dynamically relevant regions of the PES will contribute significantly, through adding points in these regions to the data set. These dynamically relevant regions are found by performing QCT calculations (see below). The new data points to be added to the PES data set are selected according to the *h-weight* criterium and (or) the *variance criterium*. Using the *h-weight* criterium,^{54,57} new points are added in the region most frequently visited by the trajectories, so long as there are not already too many data points representing this region in the PES data set. In the variance criterium,⁵⁷ it is assumed that a new added point should be in the region where the interpolation by the weighted Taylor expansions is the most inaccurate, according to a weighted mean square deviation criterium.

The procedure of adding new points to the data set in the Grow method follows the following steps:

(1) Generate an initial PES data set by employing the three-layer slab model with a (2×2) unit cell, which contains 73 data points along three different reaction paths for H_2 dissociation on the Ti/Al(100) surface. The three one-dimensional reaction paths correspond to H_2 dissociation on top Ti, top Al, and hollow sites.

(2) Using this initial PES data set, run 20 QCTs on the interpolated PES. Trajectory configurations are recorded every 50 time steps [the time step Δt is 0.01 atomic unit (a.u.)]. From these recorded trajectory configurations, new data points are selected according to the *h-weight* criterium and the *variance criterium*, alternately (i.e., the first data point is selected by the *h-weight* criterium, the next one by the *variance criterium*, and so on) and added to the data set.

(3) After repeating the above two steps under point (2), until 100 new points has been added to the PES, the reaction probability for a number of initial H_2 rovibrational states and collision energies is computed by running 5000 quasiclassical trajectories for each state and collision energy. If the reaction probability is not converged, we return to step (2) above, and continue the Grow process. Otherwise, if the reaction probabilities are converged to within a standard error of 0.70%, we stop adding new points, and the Grow process ends.

In order to have an accurate PES for the $H_2 + \text{Ti/Al(100)}$ reaction, a total number of $N_{\text{data}} = 4315$ points (4242 added points and 73 in the initial data set) are needed in the final data set. An illustration of the convergence process for two different H_2 initial states with several incident energies is shown in Fig. 2. In our case, reaction probabilities at low incident energies converge faster and have smaller errors than probabilities at higher incident energies. This phenomenon can be explained by the fact that convergence at higher energies requires sampling in a larger region of the PES, and that small probabilities computed with the QCT method and the Monte Carlo sampling have small absolute errors in them. In the non-activated system $H_2 + \text{Pd(111)}$ ⁶⁵ studied by Busnengo and co-workers, it was found that low energy trajectories can also explore large parts of the PES. In their system, 83% of the

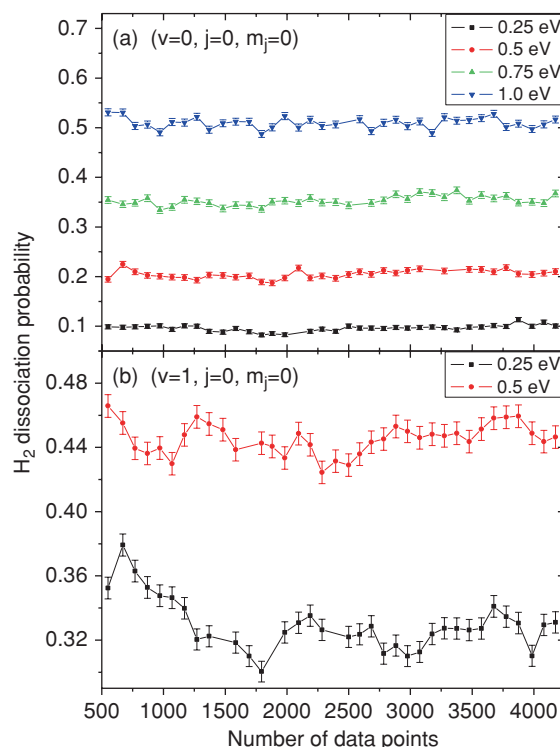


FIG. 2. (a) Grow reaction probability convergence with an error bar for the H_2 initial vibrational ground state ($v = 0$, $j = 0$). Results are shown for initial incident energies 0.25, 0.5, 0.75, and 1.0 eV. (b) The same as (a) but now results for the first vibrationally excited state ($v = 1$, $j = 0$) are shown for incident energies 0.25 and 0.50 eV. In total 4315 data points are added to the data set.

data points are added in the exit channel even at a low incident energy of 25 meV,⁶⁵ and in this aspect the $H_2 + \text{Pd(111)}$ system differs from the activated system studied here.

C. CT and QCT calculations

As already mentioned, quasiclassical trajectories were run to find and sample the dynamically relevant regions of the PES during the Grow process, and to compute reaction probabilities. The initial rovibrational energy of the $H_2(v, j, m_j)$ molecule is taken into account by sampling the initial condition of the trajectories from a microcanonical ensemble. The velocities of H-atom 1 and 2 are calculated using $\mathbf{v}_1 = \mathbf{v}_{\text{kin}} + \mathbf{v}_{\text{vib}} + \mathbf{v}_{\text{rot}}$ and $\mathbf{v}_2 = \mathbf{v}_{\text{kin}} - \mathbf{v}_{\text{vib}} - \mathbf{v}_{\text{rot}}$, respectively, in which \mathbf{v}_{kin} is the velocity in the Z direction calculated as $\sqrt{2E_{\text{kin}}/M}$, where E_{kin} is the incidence energy and M is the mass of H_2 . \mathbf{v}_{vib} (\mathbf{v}_{rot}) is the contribution to the atomic velocity due to vibration (rotation). In the QCT calculations, the vibrational zero-point energy (ZPE) with a value of 0.27 eV is modelled in the trajectories. For the cartwheel rotationally excited state ($v = 0$, $j = 4$, $m_j = 0$) and the helicopter rotationally excited state ($v = 0$, $j = 4$, $m_j = 4$), the initial energy of the trajectories also includes the rotational energy $E_{\text{rot}} = 0.14$ eV. For the first vibrationally excited state ($v = 1$, $j = 0$) the vibrational energy is set to $E_{\text{vib}} = 0.78$ eV. Normal incidence is modeled in all cases. In the CT calculations, the zero-point vibrational energy is not taken into account.

The initial vibrational motion of the two H atoms is taken according to a Morse potential.⁶⁸ Inclusion of the ZPE in the dynamics makes an adiabatic transfer of the energy from internal vibration to translation possible, a phenomenon which is called vibrational softening. Although this may lead to ZPE violation, the QCT method usually gives more accurate results for H₂–surface reactions than the purely classical method.^{11,31}

Calculations are carried out for several different initial quantum rovibrational states (v , j , m_j). The initial angular momentum is fixed according to $|L| = \sqrt{j(j+1)}$, and the orientation of the L vector is selected randomly with the constraint of

$$\cos(\theta_L) = \frac{m_j}{\sqrt{j(j+1)}}, \quad (3)$$

where θ_L is the angle between L and the Z axis (which is perpendicular to the surface).

The CT and QCT simulations are implemented in an isosceles right triangle of the (2×2) unit cell formed by two Ti atoms and one shared neighboring Al atom [Fig. 1(a)], in which the projections of the initial configurations of the trajectories on the surface are inside the surface triangle and sampled by the Monte Carlo method. The trajectories are reflected back into the triangle when they reach the boundaries, according to the boundary conditions [see Fig. 1(a)] and using the symmetry. All the initial configurations correspond to H₂ in the gas phase, with $Z = 4.0$ Å above the surface unit cell, see Fig. 1(b). The details of the sampling states, i.e., the kinetic energy E_{kin} , and the (v , j , m_j) states used to “grow” the PES are in Table I. If the final H–H distance is larger than 2.64 Å, the H₂ molecule is considered to be dissociated. Otherwise, the H₂ molecule is considered to be reflected from the surface to the gas phase when its distance to the surface in Z exceeds 4.0 Å and H₂ has a velocity pointing toward the vacuum. The reaction probability in the microcanonical

TABLE I. The quantum states of H₂ molecule that are sampled while adding data points to the PES data set using the Grow method at different kinetic energy E_{kin} (eV). The vibrational state is given by v , rotational state by j , and the magnetic rotational quantum number by m_j .

E_{kin}	v	j	m_j
0.23	0	0	0
0.23	0	4	0
0.23	0	4	4
0.50	0	0	0
0.50	0	4	0
0.50	0	4	4
0.70	0	0	0
0.90	0	0	0
0.90	0	4	0
0.90	0	4	4
1.20	0	0	0
1.20	0	4	4
1.50	0	0	0
0.00	1	0	0
0.23	1	0	0
0.40	1	0	0
0.50	1	0	0

ensemble is calculated as the ratio of the number of dissociated trajectories and the total number of trajectories run.

The strict localization of the system makes the CT and QCT methods easy to implement. However, quantum effects⁶⁹ which should be important for H₂, are not considered yet, which is the reason that we also need to calculate the H₂ dissociation probabilities by the quantum wave packet method in Subsection II D to test the accuracy of the QCT and CT methods. Because of the deep molecular adsorption well in the PES, quantum effects, such as resonances or tunneling, can be especially important for the reaction dynamics.

D. TDWP calculations

In the quantum dynamics, the six H₂ coordinates used are the hydrogen intermolecular distance r , its center of mass coordinates (X , Y , Z), the polar angle of orientation θ , and the azimuthal angle ϕ . To arrive at a quantum mechanical solution, we use the TDWP method⁶⁹ to solve the time-dependent Schrödinger equation,

$$i \frac{\partial \Psi}{\partial t} = \hat{H} \Psi. \quad (4)$$

The 6D Hamiltonian operator including the translational, vibrational, rotational, and potential energy terms is given by¹¹

$$\begin{aligned} \hat{H}_{6D} = & -\frac{1}{2M} \left(\frac{\partial^2}{\partial X^2} + \frac{\partial^2}{\partial Y^2} + \frac{\partial^2}{\partial Z^2} \right) - \frac{1}{2\mu} \frac{\partial^2}{\partial r^2} \\ & + \frac{\hat{j}^2}{2\mu r^2} + V_{6D}(X, Y, Z, r, \theta, \phi). \end{aligned} \quad (5)$$

Here, M is the mass of the H₂ molecule, and μ is the reduced mass associated with the vibrational motion. V_{6D} is the 6D Grow potential discussed in Sec. II B, with the potential energy values extended from the triangle [1/8 of the (2×2) unit cell] into the whole $(\sqrt{2} \times \sqrt{2})$ square unit cell by using appropriate displacements and rotations (according to symmetry).

In this paper, a pseudospectral method is used to propagate the wave packet, in which the Hamiltonian is symmetrically decomposed as a noncommutative form by using the split-operator (SPO) method.⁷⁰ The error per time step (Δt^3) is proportional to Δt^3 in the SPO method and it is unconditionally stable,³⁶ i.e., the maximum time step Δt is not determined by the range of eigenvalues of the Hamiltonian, but by the bandwidth of the initial wave packet.^{11,36,70}

In our implementation,³⁶ the initial wave packet is given by the formula,

$$\begin{aligned} \Psi(X, Y, Z, r, \theta, \phi) = & \Phi_{vj}(r) Y_{jm_j}(\theta, \phi) \frac{1}{\sqrt{A}} e^{i \vec{K}_0 \cdot \vec{R}} \\ & \times \int dk_z b(k_z) \frac{1}{2\pi} e^{ik_z Z}. \end{aligned} \quad (6)$$

Here, $\Phi_{vj}(r)$ and $Y_{jm_j}(\theta, \phi)$ are the H₂ vibrational and rotational eigenfunction, respectively, and v , j , and m_j are the corresponding rovibrational quantum numbers. The initial parallel motion of the wave packet along X and Y is described by $(1/\sqrt{A}) e^{i \vec{K}_0 \cdot \vec{R}}$, in which A is a normalization factor (the

surface area of the unit cell), \vec{K}_0 is the initial parallel momentum, and \vec{R} is the position vector (X , Y). The wave packet describing motion in the Z direction is a function of the initial momentum k_z , and is defined by

$$b(k_z) = \frac{2\zeta^2}{\pi} e^{-(k_{av}-k_z)^2\zeta^2 + i(k_{av}-k_z)Z_0}, \quad (7)$$

in which ζ is a width parameter, k_{av} is the average momentum in Z , and Z_0 is the center of the initial wave packet in the coordinate space.

In this paper, only normal incidence is considered and thus $\vec{K}_0 = 0$. Two initial wave packets with H_2 in its rovibrational ground state are propagated to obtain results for two kinetic energy ranges, i.e., 50–350 and 300–850 meV. More computational details are listed in Table II, and the method used is described fully in Ref. 36. The converged grid spacings for Z and r are found to be 0.15 and 0.085 a.u. in the high energy range, respectively, see Table II.

The discrete potential energy values and the wave packet are defined on the same grid. The wave function on X , Y , Z , and r represented by the discrete variable represen-

tation (DVR), effectively using a plane-wave basis-set.^{71,72} The angular momentum part of the wave function is represented by a finite basis representation (FBR), using orthogonal normalized associated Legendre polynomials as basis functions. Gauss–Legendre and Fourier transformations are used to transform the wave function from the FBR to the DVR.^{73,74} Quadratic form optical potentials⁷⁵ are employed with strength parameters such that the reflection from and transmission through the optical potential is minimal.

Finally, the wave packet is asymptotically analyzed by the Balint–Kurti formalism,^{76–79} in which the scattered wave packet is projected at $Z = Z_\infty$ onto the free particle states. The scattering probability at an incident energy E_{kin} for a transition from the initial state to the final state can be obtained from the S-matrix by

$$P_{vjm_j \rightarrow v'j'm'_jnm}(E_{kin}) = |S_{vjm_j \rightarrow v'j'm'_jnm}(E_{kin})|^2. \quad (8)$$

The reaction probability at an incident energy E_{kin} is given by summing up all the scattering probabilities and then subtracting from 1,

$$P_r(E_{kin}) = 1 - \sum_{v'j'm'_jnm} P_{vjm_j \rightarrow v'j'm'_jnm}(E_{kin}). \quad (9)$$

TABLE II. Parameters used for 6D quantum dynamics for the low energy interval wave packet (50–350 meV) and the high energy interval wave packet (300–850 meV) for the initial rovibrational ground state ($v = 0$, $j = 0$, $m_j = 0$). Both distance and time are in atomic unit (a.u.), and energies are in eV, unless indicated otherwise.

Parameters	50–350 meV	300–850 meV
Initial wave packet		
Center Z_0	9.15	9.15
v	0	0
j	0	0
m_j	0	0
Propagation time step	2.50	1.0
Total propagation time t	115 000	112 000
Scattering grid		
Range of Z Fourier grid	[0, 13.35]	[0, 13.353]
Grid spacing in Z	0.15	0.15
Range of Z optical potential	[7.05, 13.35]	[7.05, 13.35]
Strength of Z optical potential	0.01	0.05
Range of r Fourier grid	[0.41, 7.975]	[0.41, 7.975]
Grid spacing in r	0.085	0.085
Range of r optical potential	[4.15, 7.975]	[4.15, 7.975]
Strength of r optical potential	0.01	0.05
Range of X (Y) Fourier grid	[0, 7.63]	[0, 7.63]
Grid spacing X (Y)	0.186	0.186
Specular grid		
Range of Z Fourier grid	[0, 22.95]	[0, 22.95]
Grid spacing in Z	0.15	0.15
Range of Z optical potential	[12.0, 22.95]	[12.0, 22.95]
Strength of Z optical potential	0.01	0.05
Rotational basis set		
Maximum j in rotational basis	24	28
Maximum m_j in rotational basis	18	18
Analysis		
Z_∞	7.05	7.05

III. RESULTS AND DISCUSSION

A. PES obtained from the “Grow” method

Analysis of the PES topology is especially useful for the analysis of the reaction mechanism. The distribution of the points in the GROW PES data set is shown in Fig. 3. The most frequently visited region by the trajectories is found to be the entrance channel, according to the projection of the points on the (Z , r) coordinates [Fig. 3(a)]. Another projection of the data points on (X , Y) [Fig. 3(b)] shows that H_2 spends most of its time near the surface Ti atom (Ti top site). The θ anisotropy [the difference between the maximum and minimum value of $V(\theta)$ at fixed values of X , Y , Z , r , and ϕ] is 1.40 eV at the molecular adsorption well geometry and 10.80 eV at the minimum barrier geometry. In Fig. 3(c), from the ($\cos\theta$, ϕ) projection, most data points are located at the configuration where the θ angle is close to 90° , due to the large anisotropy of the potential with respect to θ (the H_2 molecule prefers to dissociate when the molecule is parallel to the surface). In contrast, the data are almost homogeneously distributed over ϕ which indicates that changing ϕ has little influence on the molecule–surface interaction. The ϕ anisotropy is 0.01 eV at the well geometry and 0.12 eV at the barrier geometry, in agreement with the distribution of the data in ϕ . With higher density of the data point distribution in these dynamically interesting regions, these regions have a higher precision of the potential.

Using the procedure introduced in Sec. II B, the 6D PES was obtained by MS interpolation. The one-dimensional potential along the MEP obtained from Grow is shown in Fig. 4. The reaction path from the gas phase to the molecular adsorption well is identical to the one obtained with the adaptive nudged elastic band (ANEb) (Ref. 80) method. However, the barrier height obtained from the Grow method is only 0.13 eV, and the barrier configuration has an angle of 15° with

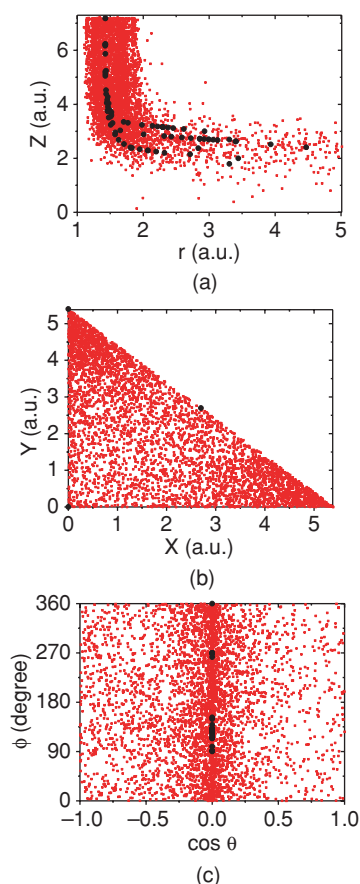


FIG. 3. Distribution of the data points: (a) projection on (Z, r) ; (b) projection on (X, Y) , where the three corners of the triangle are the same as the three corner atoms in the black triangle of Fig. 1(a); and (c) projection on $(\cos\theta, \phi)$. The black dots are the initial data points from three reaction paths with H₂ dissociating above top Ti, top Al, and hollow sites, respectively. The points indicated by black filled circles are the ones added by the Grow method. The lengths are in atomic units (a.u.).

the surface plane, with the H₂ center of mass (COM) moving away from the Ti top site by 0.55 a.u. along the Ti–Al neighboring line (or X direction). This barrier is 0.10 eV lower than the one we found in the previous paper² using ANEB calculations (see also Fig. 4). In this ANEB barrier search,

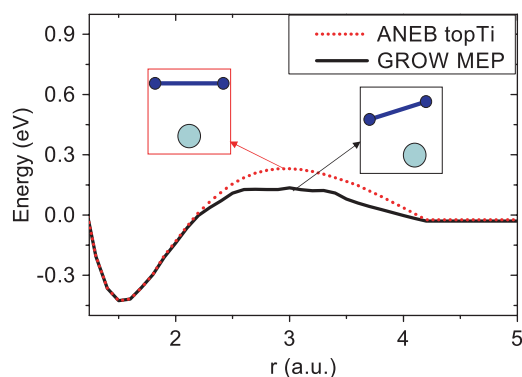


FIG. 4. Energies along the MEP as obtained from the Grow potential as shown by the solid line, as well as the reaction path for H₂ dissociating above a top Ti atom. The inset configurations illustrate that the lowest barrier geometry for H₂ dissociating along the MEP is tilted, while in the one dissociating above the Ti atom H₂ always remains parallel to the surface.

the COM of H₂ was fixed above the top Ti site and kept parallel to the surface during dissociation. However, for the lower barrier from the Grow potential, H₂ is allowed to relax freely in six DOFs, resulting in the lower barrier position: $X = 0.55$ a.u., $Y = 5.39$ a.u., $Z = 2.41$ a.u., $r = 2.92$ a.u., $\theta = 75^\circ$, and $\phi = 0^\circ$. This lower energy reaction path was first found by Valdes *et al.*⁸¹ using climbing images nudged elastic band⁸² calculations. When the COM of H₂ is restricted to be above the top Ti site,² the barrier geometry is $X = 0$ a.u., $Y = 5.39$ a.u., $Z = 2.57$ a.u., $r = 2.99$ a.u., $\theta = 90^\circ$, and $\phi = 0^\circ$, and has a barrier of 0.23 eV.

The two-dimensional (2D) cuts through the PES are shown in Fig. 5. 2D elbow plots for H₂ dissociating along the MEP and the top Ti site are shown in Figs. 5(a) and 5(b), respectively. The 2D cut along the MEP corresponds to the one-dimensional plot in Fig. 4 with a well depth of 0.43 eV and a barrier height 0.13 eV. Figures 5(c) and 5(d), show that the barrier for H₂ dissociation is much higher above the Al top site and the hollow site, respectively. In Figs. 5(e) and 5(f) 2D cuts along (X, Y) are shown, fixing r at the bond length of the molecular adsorption well value and the barrier position value while relaxing θ and ϕ , respectively. In Fig. 5(f), four potential wells (at 0.55 a.u. away from the middle of

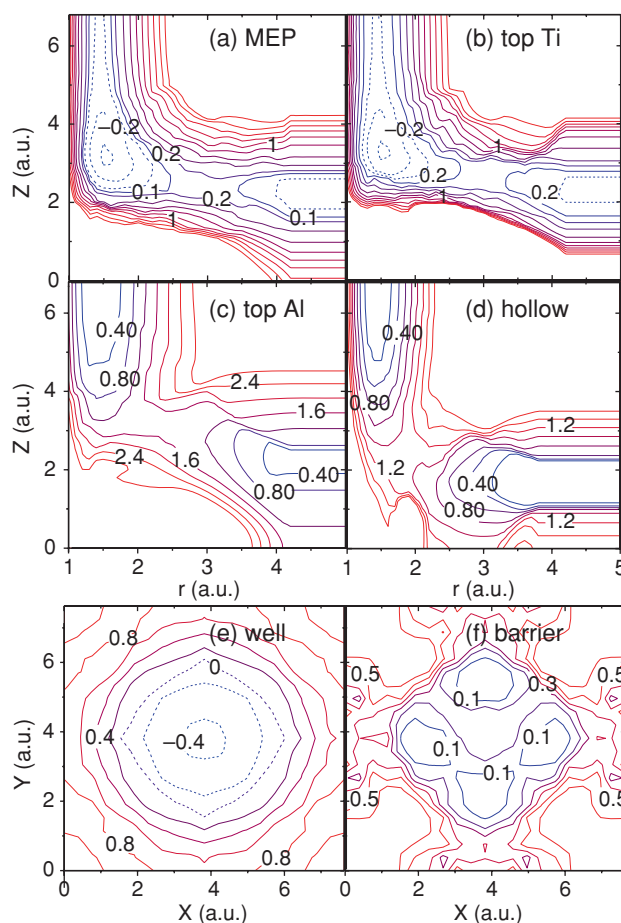


FIG. 5. (a) PES 2D cut at (Z, r) along the MEP (X, Y, θ , and ϕ are fully relaxed); (b) 2D cut at (Z, r) with COM fixed above the top Ti, $\theta = 90^\circ$ and $\phi = 0^\circ$; (c) same as (b) fixed at top Al; (d) same as (b) fixed at hollow site. Figures (e) and (f), the 2D cuts along (X, Y) when r is fixed at the well and barrier H–H distance, respectively, with relaxation of θ and ϕ .

the unit cell) can be found around the Ti atom (in the middle of the unit cell), corresponding to the barrier positions of H₂ dissociation.

B. Quasiclassical H₂ dissociation probabilities

On the PES constructed from the MS interpolation method, 6D quasiclassical dynamical trajectory calculations are performed, in which the ZPE of the H₂ molecule is considered. Reaction probabilities are obtained for the following initial H₂ states (see Fig. 6): the rovibrational ground state ($v = 0, j = 0$), the cartwheel rotationally excited state ($v = 0, j = 4, m_j = 0$), the helicopter rotationally excited state ($v = 0, j = 4, m_j = 4$), and the first vibrationally excited state ($v = 1, j = 0$). For each H₂ initial state, calculations are carried out for 100 incident energies, with equal spacing in the range from 0.03 to 1.50 eV, and for each incident energy point 5000 trajectories are run.

The QCT results in Fig. 6 show that the reaction probability increases with the incident energy except for minor fluctuations due to statistical errors. The helicopter rotationally excited state ($j = 4, m_j = 4$) has slightly higher reaction probabilities than the cartwheel rotationally excited state ($j = 4, m_j = 0$), but the differences are small, i.e., within 3.0%. Vibrational excitation has a large efficacy for promoting the reaction over the entire range of incident energies.

The distribution of mean number of rebounds (N_{reb}) counted from each QCT as a function of the collision energy, for the four different initial states, is shown in Fig. 7. A rebound occurs if the velocity of H₂ in the Z direction changes from negative to positive, thus $N_{\text{reb}} > 1$ is an indication of trapping. In Fig. 7(a), a general trend observed is that N_{reb} decreases with the increasing collision energy. N_{reb} assumes the largest values for the ($v = 0, j = 0$) state. At low collision energy ($E_{\text{kin}} = 0.10$ eV), N_{reb} is 4.66 for dissociating ($v = 0, j = 0$) H₂, the value decreasing to 1.37 at $E_{\text{kin}} = 0.90$ eV. This finding indicates that in the low energy trajectories dissociation is promoted by trapping. During this trapping,

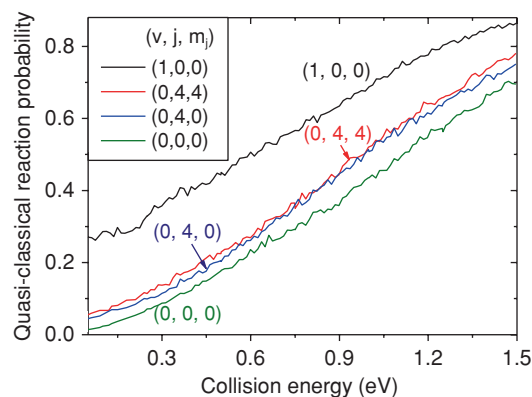


FIG. 6. Quasiclassical reaction probability for the para-H₂ rovibrational ground state ($v = 0, j = 0, m_j = 0$) (black solid line), the cartwheel rotationally excited state ($v = 0, j = 4, m_j = 0$) (dotted line), the helicopter rotationally excited state ($v = 0, j = 4, m_j = 4$) (dashed line), and the first vibrationally excited state ($v = 1, j = 0, m_j = 0$) (bold line). The collision energies are sampled from 0.03 to 1.50 eV. The error bars plotted represent one sigma interval (binomial standard deviation).

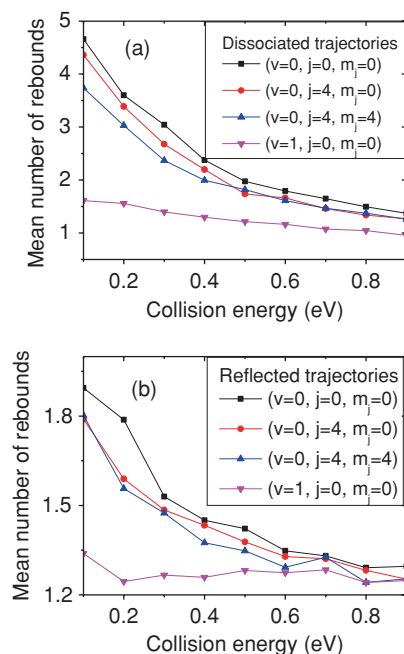


FIG. 7. Mean number of rebounds occurring in the QCTs for the reacted trajectories (a) and the reflected trajectories (b), for four initial states. A rebound occurs if the velocity in the Z direction changes from negative to positive.

configuration of the H₂ molecule can be adjusted to a proper orientation to pass the barrier. However, for large incident energy (i.e., $E_{\text{kin}} = 0.90$ eV), the majority of the trajectories have $N_{\text{reb}} = 1$. In general, the higher energy trajectories can pass the barrier with less rebounds, especially for the vibrationally excited state ($v = 1, j = 0$), see Fig. 7(a). The number of rebounds of the vibrationally excited state is relatively less sensitive to the collision energy. For this state, N_{reb} decreases from 1.85 to 0.95, for $E_{\text{kin}} = 0.10$ eV and $E_{\text{kin}} = 0.90$ eV, respectively. From the comparison of the N_{reb} values of $v = 0$ and $v = 1$, we see that $v = 1$ H₂ is more likely to dissociate with less rebounds due to its larger initial vibrational energy, i.e., it is more unlikely to be trapped in the molecular adsorption well before dissociation occurs.

The trajectories of reacting H₂ in the rotationally excited states ($j = 4, m_j = 0$) and ($j = 4, m_j = 4$) have slightly lower N_{reb} values than the ($v = 0, j = 0$) state, by about 0.30 and 0.60, respectively, when the collision energy is below 0.40 eV [see Fig. 7(a)].

For the reflected trajectories in Fig. 7(b), N_{reb} has much smaller values at low collision energy for the ($v = 0, j = 0$) rovibrational ground state, cartwheel, and helicopter rotationally excited states. At $E_{\text{kin}} = 0.10$ eV, N_{reb} of the reflected trajectories is only 1.89 for the ($v = 0, j = 0$) state [$N_{\text{reb}} = 4.66$ for dissociating ($v = 0, j = 0$) H₂]. The comparison of the two panels in Fig. 7 is consistent with the conclusion that in the less trapped trajectories H₂ is more likely to be reflected to the gas phase at low incident energies for these three states. Increasing the collisional, vibrational, and rotational energies all increase the chance of direct dissociation.

At low incident energy, trapping of the H₂ molecule is the main mechanism leading to the dissociation for the rovibrational ground state ($v = 0, j = 0$). Similar results were

previously obtained for the H₂ + Pt(211) (Refs. 37 and 83), H₂ + Pd(111) (Ref. 84), and H₂ + Pd(110) (Ref. 85) systems, in which trapping promotes reaction by providing the system with a longer time to reach an optimal configuration to overcome the barrier.

The rotational efficacy $\Theta_r(P_r)$ and the vibrational efficacy $\Theta_v(P_r)$ (Refs. 86 and 87), may be calculated from

$$\Theta_r(P_r) = \frac{E_{\text{kin}}^{j=0}(P_r) - E_{\text{kin}}^{j=4}(P_r)}{E_{\text{rot}}(j=4) - E_{\text{rot}}(j=0)},$$

$$\Theta_v(P_r) = \frac{E_{\text{kin}}^{v=0}(P_r) - E_{\text{kin}}^{v=1}(P_r)}{E_{\text{vib}}(v=1) - E_{\text{vib}}(v=0)}. \quad (10)$$

Here, E_{kin}^j (E_{kin}^v) is the translational energy required to obtain a reaction probability P_r when the H₂ molecule is initially in the rotational (vibrational) state v (j), and E_{rot} (E_{vib}) is the rotational (vibrational) energy of the H₂ molecule in the gas phase. An efficacy value of $\Theta_r(P_r)$ [$\Theta_v(P_r)$] larger than 1.0 means that putting energy into rotation (vibration) is more efficient at promoting reaction than putting energy into translation. The opposite is true for a values less than 1.0.

Using these two formulae, both the rotational and vibrational efficacy can be obtained from the reaction probability curves in Fig. 6. In the entire energy reaction range considered, the rotational efficacy $\Theta_r(P_r)$ is close to 1.0, for both the cartwheel and the helicopter rotationally excited states. This means that rotational energy is as effective at promoting the dissociation as translational energy. The vibrational efficacy is also close to 1.0 in the entire energy reaction range. However, $\Theta_v(P_r) = 1.20$ when the dissociation probability is below 30.0%, which indicates that putting energy into vibration could make the H₂ molecule circumvent the barrier in a more efficient way than possible by putting energy into translation. The vibrational efficacy decreases with the increasing dissociation probability. At a dissociation probability of 50.0%, the $\Theta_v(P_r)$ is around 1.0.

The reaction probability curves are replotted in Fig. 8 as a function of the total (internal and translational) energy. From this figure, it is seen that the H₂ dissociation probably mainly depends on the total energy and less on how the energy is divided between translation, rotation, and vibration.

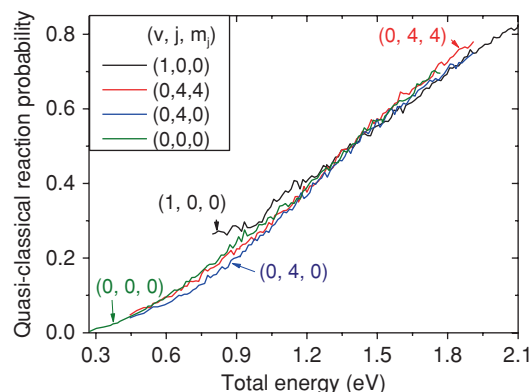


FIG. 8. Reaction probability computed with quasiclassical dynamics but plotted as a function of the total (internal and translational) energy.

The fact that the H₂ + Ti/Al(100) system, which has a deep well in front of the barrier, has a rotational and vibrational efficacy close to 1.0 suggests that the total (internal and translational) energy undergoes complete randomization in the initial conditions (translational, rotational, and vibrational energy), making the reaction rate solely dependent on the energy. This agrees with the microcanonical unimolecular rate theory of dissociative chemisorption for CH₄ on Ni(100) developed by Harrison and co-workers,²² suggesting that it should be possible to compute accurate reaction rates with this theory.

C. Quantum dynamics of H₂ dissociation probability

Quantum dynamical calculations on the H₂ + Ti/Al(100) reaction have been carried out for normal incidence of H₂ in its ($v = 0, j = 0, m_j = 0$) state.

The converged quantum reaction probability for H₂ dissociation is plotted in Fig. 9. Corresponding quasiclassical and pure classical reaction probabilities (the latter one with $E_{\text{vib}} = 0$ eV) are also shown in this figure. The quantum reaction probability shows fluctuations in the low energy range, which may be explained by resonances (the molecule has extra time to tunnel through the barrier when trapped in a metastable state leading to dissociation at the corresponding energies). The results of the quantum dynamics calculation agree well with the quasiclassical ones in the low energy interval 50–200 meV, but the quantum dissociation probability are higher than the quasiclassical results by up to 0.06 (corresponding to a relative difference of 30.0%) for incident energies larger than 200 meV. The difference between quasiclassical and quantum reaction probabilities presumably tells us that the randomization of the energy in a quasiclassical trajectory may hinder the H₂ dissociation, especially at high incident energies. Classical dynamics results (see Fig. 9) show a reaction probability that is zero when E_{kin} is below 0.20 eV.

To illustrate the development of the wave function in time, the projected probability density on the 2D (Z, r) grid is shown in Fig. 10. In the high energy range [Figs. 10(a–f)], the most interesting phenomenon found from the propagation of the wave packet is that a node clearly appears in r when the propagation time $t = 4000$ a.u. [Fig. 10(d)] and this node remains during the process of propagation. At $t = 6000$ a.u.,

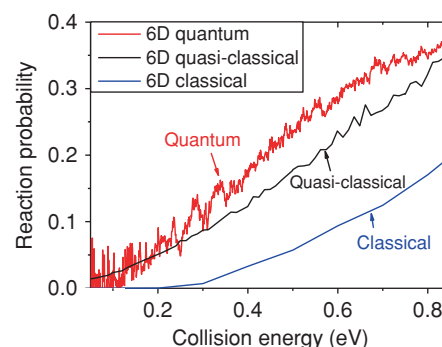


FIG. 9. Quantum reaction probability for H₂ initially in its ground rovibrational state ($v = 0, j = 0, m_j = 0$). The quasiclassical and the classical results are also plotted.

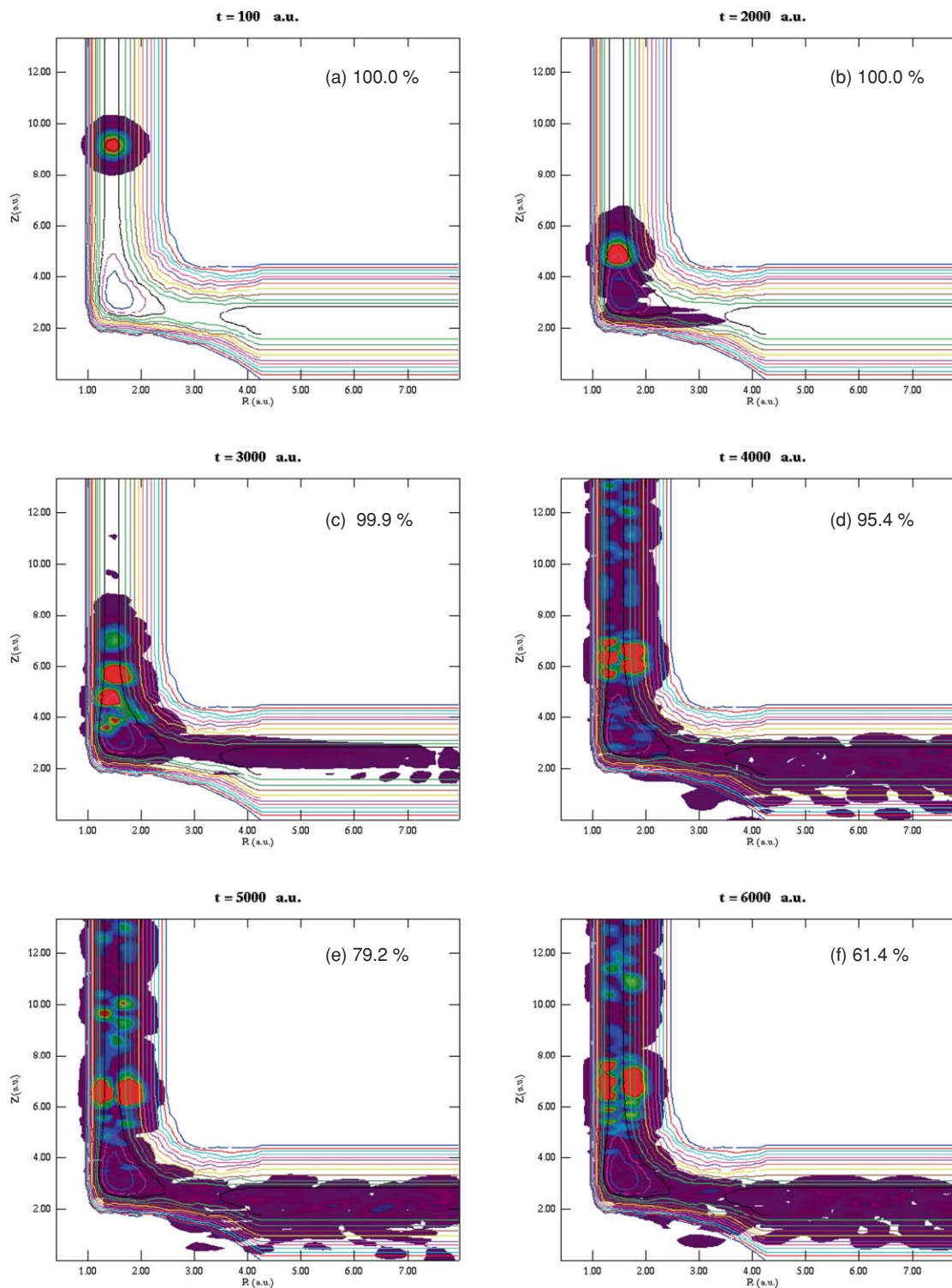


FIG. 10. Snapshots of the TDWP probability density as a function of Z and r for different propagation times in the range 100–12500 a.u., for the high collision energy range 300–850 meV. The probability density is given by $\Psi(Z, r)\Psi(Z, r)^*$, in which the $\Psi(Z, r)$ is the projection of the 6D wave packet on 2D (Z, r) grid for $(j' = 0, m'_j = 0, n' = 0, m' = 0)$. The background of the plot is the 2D PES along the MEP, shown in Fig. 5(a).

only the $v' = 1$ state can be observed in the entrance channel, and at this time 61.4% of the norm of the wave packet is still present in the strong interaction region (entrance channel and the molecular adsorption well) of the scattering grid. Although, $P(v = 0, j = 0 \rightarrow v' = 1)$ is only 6.0%, the results suggest that trapping in the molecular adsorption well can arise from the vibrational excitation of H_2 .

IV. CONCLUSIONS

In this paper, based on the density functional theory, we studied the elementary reaction of H_2 dissociation on a one ML Ti covered Al(100) surface. First, the Grow method is applied to build a 6D electronic ground state PES using the BO and static surface approximations. H_2 dissociation

probabilities are calculated through both the CT and QCT methods and the TDWP method. The dynamically interesting region is found to be at the Ti site of the surface where the molecular adsorption well in the MEP is located, leading to a high density of data points in this region with the Grow method. The MEP has been improved in the Grow PES. The new H₂ dissociation barrier is found to be 0.13 eV, which is 0.10 eV lower than the one reported in our previous paper.²

In the quasiclassical dynamics, we have calculated the dissociation probabilities for four initial quantum states of H₂, i.e., ($v = 0, j = 0$), ($v = 0, j = 4, m_j = 0$), ($v = 0, j = 4, m_j = 4$), and the vibrationally excited state ($v = 1, j = 0$). The dissociated trajectories for low incident energies (i.e., below 0.20 eV) of the rovibrational ground state and the rotationally excited states have relatively large N_{reb} values (between 3 and 5), which indicates that these trajectories are trapped before dissociation. In contrast, the molecule in its vibrationally excited state dissociates more directly. Both rotational and vibrational excitation promote direct H₂ dissociation efficiently, with an efficacy of approximately 1.

The presence of the deep adsorption well in front of the barrier leads to statistical behavior: the H₂ dissociation probability depends only on the total (internal and translational) energy, except that the vibrational efficacy is larger than 1.0 in the low reaction probability region.

The reaction of H₂ in its rovibrational ground state ($v = 0, j = 0$) is also considered using quantum dynamics. The calculations show that the QCT method describes the reaction more accurately than the CT method, as found earlier for most H₂ + metal surface systems studied.

In summary, based on the evidence that Ti plays a role in the process of hydrogen storage in NaAlH₄, we theoretically calculated the H₂ dissociation probability on a one ML Ti covered Ti/Al(100) surface. We hope that our predictions of the reaction probability curves can be confirmed by molecular beam experiments.

ACKNOWLEDGMENTS

The research of J.C.C. is supported by the Marie Curie Research Training Network HYDROGEN. He is grateful for invaluable help to A. Valdés de Luxán, G. P. Krishnamohan, A. Marashdeh, I. M. N. Groot, T. P. M. Goumans, and M. C. van Hemert. We acknowledge the Stichting Nationale Computerfaciliteiten (NCF) for a grant of computer time.

- ¹B. Bogdanovic and M. Schwickardi, *J. Alloys Compd.* **253**, 1 (1997).
- ²J.-C. Chen, J. C. Juanes-Marcos, A. Al-Halabi, R. A. Olsen, and G.-J. Kroes, *J. Phys. Chem. C* **113**, 11027 (2009).
- ³J. P. Cowin, C.-F. Yu, S. J. Sibener, and J. E. Hurst, *J. Chem. Phys.* **75**, 1033 (1981).
- ⁴J. E. Lennard-Jones and A. F. Devonshire, *Nature (London)* **137**, 1069 (1936).
- ⁵R. B. Gerber, *Chem. Rev.* **87**, 29 (1987).
- ⁶C. Chakravarty and H. Metiu, *J. Chem. Phys.* **102**, 8643 (1995).
- ⁷E. J. Rackham, T. Gonzalez-Lezana, and D. E. Manolopoulos, *J. Chem. Phys.* **119**, 12895 (2003).
- ⁸W. H. Miller, *J. Chem. Phys.* **52**, 543 (1970).
- ⁹J. C. Juanes-Marcos, A. J. C. Varandas, and S. C. Althorpe, *J. Chem. Phys.* **128**, 211101 (2008).
- ¹⁰G. O. Sitz, *Rep. Prog. Phys.* **65**, 1165 (2002).
- ¹¹G.-J. Kroes, *Prog. Surf. Sci.* **60**, 1 (1999).

- ¹²A. Hodgson, J. Moryl, P. Traversaro, and H. Zhao, *Nature (London)* **356**, 501 (1992).
- ¹³C. T. Rettner, D. J. Auerbach, and H. A. Michelsen, *Phys. Rev. Lett.* **68**, 1164 (1992).
- ¹⁴G. R. Darling and S. Holloway, *J. Chem. Phys.* **97**, 734 (1992).
- ¹⁵G. R. Darling and S. Holloway, *Surf. Sci.* **307–309**, 153 (1994).
- ¹⁶H. A. Michelsen, C. T. Rettner, D. J. Auerbach, and R. N. Zare, *J. Chem. Phys.* **98**, 8294 (1993).
- ¹⁷C. T. Rettner, H. A. Michelsen, and D. J. Auerbach, *J. Chem. Phys.* **102**, 4625 (1995).
- ¹⁸C. Díaz, E. Pijper, R. A. Olsen, H. F. Busnengo, D. J. Auerbach, and G.-J. Kroes, *Science* **326**, 832 (2009).
- ¹⁹C. Díaz, R. A. Olsen, D. J. Auerbach, and G.-J. Kroes, *Phys. Chem. Chem. Phys.* **12**, 6499 (2010).
- ²⁰S. J. Guldung, A. M. Wodtke, H. Hou, C. T. Rettner, H. A. Michelsen, and D. J. Auerbach, *J. Chem. Phys.* **105**, 9702 (1996).
- ²¹H. Hou, S. J. Guldung, C. T. Rettner, A. M. Wodtke, and D. J. Auerbach, *Science* **277**, 80 (1997).
- ²²H. L. Abbott, A. Bukoski, and I. Harrison, *J. Chem. Phys.* **121**, 3792 (2004).
- ²³P. Nieto, E. Pijper, D. Barredo, G. Laurent, R. A. Olsen, E.-J. Baerends, G.-J. Kroes, and D. Farías, *Science* **312**, 86 (2006).
- ²⁴G.-J. Kroes, G. Wiesenekker, E.-J. Baerends, and R. C. Mowrey, *Phys. Rev. B* **53**, 10397 (1996).
- ²⁵A. Gross, S. Wilke, and M. Scheffler, *Phys. Rev. Lett.* **75**, 2718 (1995).
- ²⁶J. Dai and J. C. Light, *J. Chem. Phys.* **107**, 1676 (1997).
- ²⁷J. Dai and J. C. Light, *J. Chem. Phys.* **107**, 8432 (1997).
- ²⁸J. Dai and J. C. Light, *J. Chem. Phys.* **108**, 7816 (1998).
- ²⁹A. Gross, *Surf. Sci. Rep.* **32**, 291 (1998).
- ³⁰G.-J. Kroes, E.-J. Baerends, and R. C. Mowrey, *Phys. Rev. Lett.* **78**, 3583 (1997).
- ³¹G.-J. Kroes and M. F. Somers, *J. Theor. Comput. Chem.* **4**, 493 (2005).
- ³²SARA, <http://www.sara.nl>.
- ³³A. Eichler, J. Halfner, A. Gross, and M. Scheffler, *Chem. Phys. Lett.* **311**, 1 (1999).
- ³⁴A. Dianat and A. Gross, *J. Chem. Phys.* **120**, 5339 (2004).
- ³⁵G.-J. Kroes, E.-J. Baerends, and R. C. Mowrey, *Phys. Rev. Lett.* **78**, 3583 (1998).
- ³⁶E. Pijper, G.-J. Kroes, R. A. Olsen, and E.-J. Baerends, *J. Chem. Phys.* **117**, 5885 (2002).
- ³⁷R. A. Olsen, D. A. McCormack, M. Luppi, and E.-J. Baerends, *J. Chem. Phys.* **128**, 194715 (2008).
- ³⁸H. F. Busnengo, E. Pijper, M. F. Somers, G.-J. Kroes, A. Salin, R. A. Olsen, D. Lemoine, and W. Dong, *Chem. Phys. Lett.* **356**, 515 (2002).
- ³⁹J. K. Vincent, R. A. Olsen, G.-J. Kroes, M. Luppi, and E.-J. Baerends, *J. Chem. Phys.* **122**, 044701 (2005).
- ⁴⁰P. Rivière, M. F. Somers, G.-J. Kroes, and F. Martín, *Phys. Rev. B* **73**, 205417 (2006).
- ⁴¹A. Gross and M. Scheffler, *Phys. Rev. B* **61**, 8425 (2000).
- ⁴²I. M. N. Groot, J. C. Juanes-Marcos, C. Díaz, M. F. Somers, R. A. Olsen, and G.-J. Kroes, *Phys. Chem. Chem. Phys.* **12**, 1331 (2010).
- ⁴³P. Hohenberg and W. Kohn, *Phys. Rev.* **136**, B864 (1964).
- ⁴⁴W. Kohn and L. J. Sham, *Phys. Rev.* **140**, A1133 (1965).
- ⁴⁵DACAPO, See <https://wiki.fysik.dtu.dk/dacapo/Dacapo>.
- ⁴⁶J. P. Perdew, J. A. Chevary, S. H. Vosko, K. A. Jackson, M. R. Pederson, D. J. Singh, and C. Fiolhais, *Phys. Rev. B* **46**, 6671 (1992).
- ⁴⁷P. Rivière, H. F. Busnengo, and F. Martín, *J. Chem. Phys.* **121**, 751 (2004).
- ⁴⁸D. Vanderbilt, *Phys. Rev. B* **41**, 7892 (1990).
- ⁴⁹H. Monkhorst and D. Pack, *Phys. Rev. B* **13**, 5188 (1976).
- ⁵⁰J. P. Perdew, K. Burke, and M. Ernzerhof, *Phys. Rev. Lett.* **77**, 3865 (1996).
- ⁵¹B. Hammer, L. B. Hansen, and J. K. Nørskov, *Phys. Rev. B* **59**, 7413 (1999).
- ⁵²I. M. N. Groot, H. Ueta, M. J. T. C. van der Niet, A. W. Kleyn, and L. B. F. Juurlink, *J. Chem. Phys.* **127**, 244701 (2007).
- ⁵³G. A. Bocan, R. Díez Muiño, M. Alducin, H. F. Busnengo, and A. Salin, *J. Chem. Phys.* **128**, 154704 (2008).
- ⁵⁴J. Ischtwan and M. A. Collins, *J. Chem. Phys.* **100**, 8080 (1994).
- ⁵⁵K. C. Thompson, M. J. T. Jordan, and M. A. Collins, *J. Chem. Phys.* **108**, 8302 (1998).
- ⁵⁶R. P. A. Bettens and M. A. Collins, *J. Chem. Phys.* **111**, 816 (1999).
- ⁵⁷M. A. Collins, *Theor. Chem. Acc.* **108**, 313 (2002).
- ⁵⁸C. Crespos, M. A. Collins, E. Pijper, and G.-J. Kroes, *J. Chem. Phys.* **120**, 2392 (2004).

- ⁵⁹C. Crespos, M. A. Collins, E. Pijper, and G.-J. Kroes, *Chem. Phys. Lett.* **376**, 566 (2003).
- ⁶⁰C. Díaz, R. A. Olsen, H. F. Busnengo, and G.-J. Kroes, *J. Phys. Chem. C* **114**, 11192 (2010).
- ⁶¹H. F. Busnengo, A. Salin, and W. Dong, *J. Chem. Phys.* **112**, 7641 (2000).
- ⁶²R. A. Olsen, H. F. Busnengo, A. Salin, M. F. Somers, G.-J. Kroes, and E.-J. Baerends, *J. Chem. Phys.* **116**, 3814 (2002).
- ⁶³C. Díaz, J. K. Vincent, G. P. Krishnamohan, R. A. Olsen, G.-J. Kroes, K. Honkala, and J. K. Nørskov, *J. Chem. Phys.* **125**, 114706 (2006).
- ⁶⁴C. Díaz, J. K. Vincent, G. P. Krishnamohan, R. A. Olsen, G.-J. Kroes, K. Honkala, and J. K. Nørskov, *Phys. Rev. Lett.* **96**, 096102 (2006).
- ⁶⁵P. N. Abufager, C. Crespos, and H. F. Busnengo, *Phys. Chem. Chem. Phys.* **9**, 2258 (2007).
- ⁶⁶G. P. Krishnamohan, R. A. Olsen, G.-J. Kroes, F. Gatti, and S. Woittequand, *J. Chem. Phys.* **133**, 144308 (2010).
- ⁶⁷K. G. Prasanna, R. A. Olsen, A. V. de Luxán, and G.-J. Kroes, *Phys. Chem. Chem. Phys.* **12**, 7654 (2010).
- ⁶⁸E. Castro, P. Martín, and J. L. Paz, *Phys. Lett. A* **364**, 135 (2007).
- ⁶⁹R. Kosloff, *J. Phys. Chem.* **92**, 2087 (1988).
- ⁷⁰M. D. Feit, J. A. Fleck, and A. Steiger, *J. Comput. Phys.* **47**, 412 (1982).
- ⁷¹J. V. Lill, G. A. Parker, and J. C. Light, *Chem. Phys. Lett.* **89**, 483 (1982).
- ⁷²J. C. Light, I. P. Hamilton, and J. V. Lill, *J. Chem. Phys.* **82**, 1400 (1985).
- ⁷³G. C. Corey and D. Lemoine, *J. Chem. Phys.* **97**, 4115 (1992).
- ⁷⁴D. Lemoine, *J. Chem. Phys.* **101**, 10526 (1994).
- ⁷⁵A. Vibok and G. G. Balint-Kurti, *J. Phys. Chem.* **96**, 8712 (1992).
- ⁷⁶G. G. Balint-Kurti, R. N. Dixon, and C. C. Marston, *J. Chem. Soc., Faraday Trans.* **86**, 1741 (1990).
- ⁷⁷C. C. Marston, G. G. Balint-Kurti, and R. N. Dixon, *Theor. Chim. Acta* **79**, 313 (1991).
- ⁷⁸G. G. Balint-Kurti, R. N. Dixon, and C. C. Marston, *Int. Rev. Phys. Chem.* **11**, 317 (1992).
- ⁷⁹R. C. Mowrey and G.-J. Kroes, *J. Chem. Phys.* **103**, 1216 (1995).
- ⁸⁰G. Henkelman and H. Jónsson, *J. Chem. Phys.* **113**, 9978 (2000).
- ⁸¹A. V. de Luxán, A. Arnaldsson, and H. Jónsson, (unpublished).
- ⁸²G. Henkelman, B. Uberuaga, and H. Jónsson, *J. Chem. Phys.* **113**, 9901 (2000).
- ⁸³R. A. Olsen, D. A. McCormack, and E.-J. Baerends, *Surf. Sci. Lett.* **517**, L325 (2004).
- ⁸⁴H. F. Busnengo, C. Crespos, W. Dong, J. C. Rayez, and A. Salin, *J. Chem. Phys.* **116**, 9005 (2002).
- ⁸⁵M. A. Di Césare, H. F. Busnengo, W. Dong, and A. Salin, *J. Chem. Phys.* **118**, 11226 (2003).
- ⁸⁶G.-J. Kroes, G. Wiesenekker, E.-J. Baerends, R. C. Mowrey, and D. Neuhauser, *J. Chem. Phys.* **105**, 5979 (1996).
- ⁸⁷C. Díaz and R. A. Olsen, *J. Chem. Phys.* **130**, 094706 (2009).